Proceedings of ASME TURBO EXPO 2003
Power for Land, Sea, and Air
June 16-19, Atlanta, Georgia, USA

GT2003-38252

COMPUTATIONAL PREDICTIONS OF ENDWALL FILM-COOLING FOR A FIRST STAGE VANE

Daniel G. Knost and Karen A. Thole
Mechanical Engineering Department
Virginia Polytechnic Institute and State University
Blacksburg, VA 24061

ABSTRACT

In gas turbine development, the direction has been higher turbine inlet temperatures to increase the work output and thermal efficiency. This extreme environment can significantly impact component life. One means of preventing component burnout in the turbine is to effectively use film-cooling whereby coolant is extracted from the compressor and injected through component surfaces. One such surface is the endwall of the first stage nozzle guide vane. This paper presents results from a computational study of two endwall film-cooling hole patterns combined with cooling from a flush slot that simulates leakage between the combustor and turbine sections. Results indicate reasonable agreement between predictions and measurements of the turbine endwall cooling for a flush slot alone. Effectiveness predictions showed an increase in film-cooling flow was needed for both hole patterns to insure coolant was present near the pressure side of the vane. Results also indicated that superposition overpredicted the effectiveness levels along the endwall for the combined endwall film-cooling and slot cooling configurations.

INTRODUCTION

Given the huge number of sustained operational hours required for industrial turbines, two important demands are component life and overall engine performance. These demands are somewhat conflicting because high temperatures are needed at the entrance to the turbine for good performance, which in turn cause reduced component life. With the high temperature demands, one critical region in an engine is the endwall of the first turbine vane. Many vane endwall designs have film-cooling holes to help reduce the impact of the thermal environment.

Turbine designers generally have difficulty choosing the placement of these cooling holes and, as such, many designs are dependent upon past engine experience. The local thermal environment for the endwall is dictated by the secondary flows that develop through the vane passage. Secondary flows, which typically include leading edge and passage vortices, are dictated by the geometrical features of the vane itself, the vane-endwall juncture geometry, and combustor exit conditions. Most combustor-turbine junctions have slots through which coolant leaks into the main gas path. These junctions, depending on the design and operating conditions, typically consist of either a backward-facing slot, a forward-facing slot, or a flush slot. The coolant flow from the slot influences the total pressure profile exiting the combustor and may span as much as 10-15% of the span for both the inner and outer radii platforms of the first vane. In turn, this total pressure profile in the near-platform region dictates the development of the secondary flows through the vane passage.

To improve the understanding of this complex interaction between the combustor-turbine interface and the downstream endwall film-cooling flows, a number of CFD simulations were completed. First, a set of simulations was completed to compare with experimental data in which coolant was injected from a slot that was flush with the endwall surface. After this benchmark, a number of simulations were evaluated to determine the adiabatic effectiveness on the vane platform due to the following cooling schemes: i) coolant injection from an upstream flush slot alone; ii) coolant injection from two different endwall cooling hole patterns; and iii) coolant injection from a combined flush slot and endwall cooling holes. In particular, this study determines the effect that the coolant from the flush slot had on the downstream endwall cooling.

SUMMARY OF PAST LITERATURE

There have been a number of studies documenting endwall film-cooling and a number of studies documenting cooling from the turbine-combustor junction. As will also be discussed in this summary, there has been only one study presented in the literature that has combined endwall film-cooling with coolant leakage from an upstream slot.

The most recent studies of detailed endwall film cooling have been those conducted by Friedrichs et al. [1, 2, and 3]. The results of their first study [1], which were all surface measurements or visualization, indicated a strong influence of the secondary flows on the film cooling and an influence of the film-cooling on the secondary flows. Quite counter-intuitive to most, their data showed that the angle at which the coolant leaves the hole did not dictate the coolant trajectory except near

the hole exit. Furthermore the endwall cross-flow was altered so that the cross-flow was turned toward the inviscid streamlines, which was due to the film-cooling injection.

There have been a few studies that have measured endwall heat transfer as a result of injection from a two-dimensional, flush slot just upstream of the vane. Blair [4] measured adiabatic effectiveness levels and heat transfer coefficients for a range of blowing ratios through a flush slot placed just upstream of the leading edges of his single passage channel. One of the key findings was that the endwall adiabatic effectiveness distributions showed extreme variations across the vane gap. Much of the coolant was swept across the endwall toward the suction side corner resulting in reduced coolant near the pressure side. As the blowing ratio was increased, he found that the extent of the coolant coverage also increased. Measured heat transfer coefficients were similar between no slot and slot injection cases. In a later study by Granser and Schulenberg [5], similar adiabatic effectiveness results were reported with higher values occurring near the suction side of the vane.

A series of experiments have been reported for various injection schemes upstream of a nozzle guide vane with a contoured endwall by Burd and Simon [6]; Burd et al. [7]; Oke, et al. [8] and Oke et al. [9]. In the studies presented by Burd and Simon [6], Burd et al. [7] and Oke, et al. [8] coolant was injected from an interrupted, flush slot that was inclined at 45° just upstream of their vane. Similar to others, they found that most of the slot coolant was directed toward the suction side at low slot flow conditions. As they increased the percentage of slot flow to 3.2% of the exit flow, however, their measurements indicated better coverage occurred between the airfoils. In contrast, the study by Oke et al. [9] used a double row of film-cooling holes that were aligned with the flow direction and inclined at 45° with respect to the surface while maintaining nearly the same optimum 3% bleed flow of their previously described studies. They found that the jets lifted off the surface producing more mixing thereby resulting in a poorer thermal performance than the single slot.

Roy et al. [10] compared their experimental measurements and computational predictions for a flush cooling slot that extended over only a portion of the pitch directly in front of the vane stagnation. Contrary to the previously discussed studies, their adiabatic effectiveness measurements indicated that the coolant migrated toward the pressure side of the vane. Their measurements indicated reduced values of local heat transfer coefficients at the leading edge when slot cooling was present relative to no slot cooling.

Colban et al. [11, 12] reported flow field and endwall effectiveness contours for a backward-facing slot with several different coolant exit conditions. Their results indicated the presence of a tertiary vortex that developed in the vane passage due to a peaked total pressure profile in the near-wall region. For all of the conditions simulated, the effectiveness contours indicated the coolant from the slot was swept towards the suction surface. While this study was completed for the same vane geometry as that reported in our paper, the slot geometry has been altered to be flush with the endwall surface.

The only studies to have combined an upstream slot with film-cooling holes in the downstream endwall vane passage were those of Kost and Nicklas [13] and Nicklas [14]. One of the most interesting results from this study was that they found for the slot flow alone, which was 1.3% of the passage mass flow, the horseshoe vortex became more intense. This increase in intensity resulted in the slot coolant being moved off of the endwall surface and heat transfer coefficients that were over three times that measured for no slot flow injection. They attributed the strengthening of the horseshoe vortex to the fact that for the no slot injection the boundary layer was already separated with fluid being turned away from the endwall at the injection location. Given that the slot had a normal component of velocity, injection at this location promoted the separation and enhanced the vortex. Their adiabatic effectiveness measurements indicated higher values near the suction side of the vane due to the slot coolant migration.

Clearly there is a need for further study on the cooling problems associated with the endwall of a turbine platform. Our study focuses on the interaction between the coolant leaving a two-dimensional slot at the combustor-turbine interface and the endwall film-cooling injection.

DESIGN OF ENDWALL COOLING SCHEMES

As was stated in the literature review, there is a lack of knowledge concerning the combination of a leakage slot flow with endwall film-cooling holes. As such, two realistic cooling hole patterns were developed based upon industry input, as shown in Figures 1a-1b. A number of holes have been numbered for the two patterns, which will be referred to later in our paper, as shown in Figure 1a. Iso-velocity contours and injection directions are shown in Figure 1b. Also shown in Figure 1b is the location of a gutter, which is the joint between the two mating platforms. The gutter has the potential of having coolant leakage as well, but was not simulated in our studies. Table 1 provides a summary of parameters relevant to both cooling scheme designs. The airfoil geometry used in the current study is a commercial, first-stage, stator vane previously described by Radomsky and Thole [15]. The vane is two-dimensional with the midspan cross-section modeled along the entire span.

Both cooling hole patterns included a two-dimensional flush slot located $0.31C_a$ upstream of the vane stagnation, representing the combustor-turbine interface. The slot injected at an angle of 45˚ with respect to the endwall and had a slot length (flowpath length) to width (cross-sectional width) of 1.8.

Downstream of the slot, two different endwall cooling hole patterns were placed. All film-cooling holes injected at an angle of 30˚ with respect to the endwall surface. For both of the hole patterns the film-cooling holes were located in two distinct regions: the leading edge region and between the airfoils. The leading row of film-cooling holes located between the airfoils injected at a compound angle of 90˚ with respect to the inlet flow angle (as indicated by arrows in Figure 1b) and were spaced four hole diameters apart. The holes located directly upstream of the vane injected in the inlet flow direction and were spaced three hole diameters apart. The only difference between the two endwall cooling configurations in the leading edge region was the presence of a gap between the 90˚ holes in hole pattern #2 as compared with a continuous row of holes for hole pattern #1. This gap for hole pattern #2 was present due to the gutter design.

Harasgama and Burton [16] suggested that locating film-cooling holes along iso-mach lines would ensure a uniform blowing rate and momentum flux helping to prevent jet lift off. Hole pattern #1 was designed such that the cooling holes were located along straight lines approximating the iso-velocit

contours. Iso-velocity contours were chosen because experiments will be conducted in a low speed facility with little variation in Mach number. Hole pattern #2 was designed such that the holes nearest to the pressure side of the vane lie on the same iso-velocity contours that were used in hole pattern #1,

Table 1. Summary of Geometrical Cooling Features

Feature	9X Scale
Cooling hole diameter (cm)	0.46
Cooling Hole L/D	8.3
Hole injection angle	30˚
P/D for leading edge holes	4 / 3
P/D for passage holes	3
Slot width (cm)	1.48
Slot length to width	1.8
Upstream slot location of vane	-0.31C_a
Slot injection angle	45˚

but with the difference being the row of holes was placed along axial lines rather than iso-velocity contours. All holes in pattern #2, with the exception of two holes at the trailing edge, inject in the axial direction. The two holes at the trailing edge inject at a compound angle of 45˚. All cooling holes in each row within the passage for both patterns were spaced three hole diameters apart and injected in the axial direction.

COMPUTATIONAL AND EXPERIMENTAL METHODS

Computations were performed for incompressible, viscous, low-speed conditions with an exit Reynolds number of Re_{ex} = $1.2x10^6$ for the vane. The simulations were performed using the FLUENT commercial software package [17].

FLUENT/UNS is a pressure-based incompressible flow solver for unstructured meshes. The Reynolds Averaged Navier Stokes (RANS) equations as well as the energy and turbulence equations were solved using second-order discretization. The turbulence model that was used was an

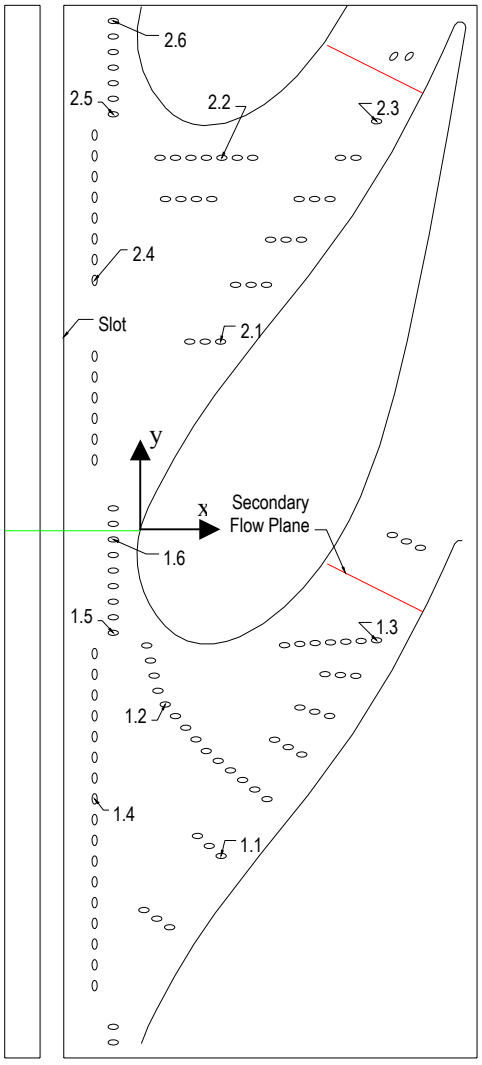

Figure 1a. The two film-cooling patterns that were simulated in this study (Pattern #1 and #2) and labels for several specific film cooling holes. In addition, a secondary flow plane is identified that was used to evaluate the flow field.

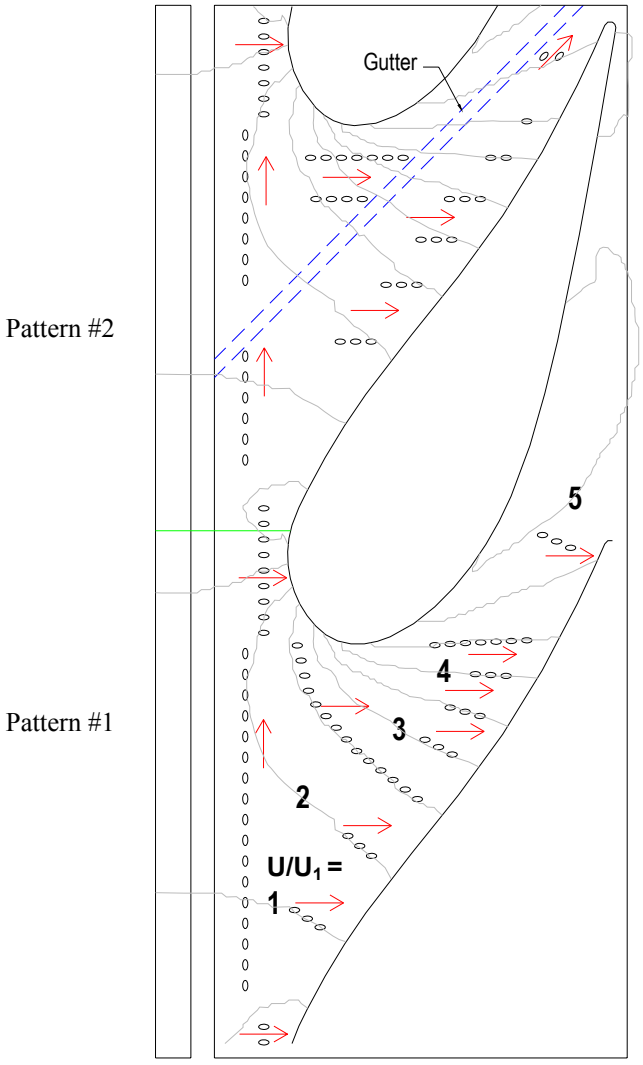

Figure 1b. Shown are the directions of the coolant hole injection along with iso–velocity contours (U/U_1) and the gutter location for mating two turbine vane platforms.

RNG κ–ε model with non-equilibrium wall-functions. Hermanson and Thole [18] were able to show good agreement between computational predictions and experimental measurements of secondary flows using this same modeling technique. FLUENT/UNS allows for unstructured meshing capability and also allows solution-adaptive mesh refinement in order to resolve regions of high gradients.

The vane and upstream contraction were modeled for these studies as shown in Figure 2a. As most combustor geometries include a contraction upstream of the turbine section, these calculations also considered a contraction, which only contracted in the spanwise (radial) direction. The start of the contraction was 1.53 true vane chords upstream of the vane stagnation with a contraction angle of 15.6˚. This contraction was designed to match future wind tunnel experiments.

The computational models were such that the vane was divided at the stagnation point and the trailing edge with a single passage being modeled. In all, five different geometric models were meshed that included the following: slot alone; hole pattern #1 and #2 alone; and combined slot with the two hole patterns. The vane was modeled from the endwall to the mid-span with boundary conditions of no-slip and symmetry, respectively. Periodic boundary conditions were placed along the pitchwise boundaries. Uniform velocity and temperature profiles were assumed at the inlet to the computational domain while an outflow boundary condition was placed 1.5C downstream of the trailing edge. The velocity contours at the end of the contraction are shown in Figure 2b. Low freestream turbulence levels were considered for this study, which is relevant to industrial based turbines which have no combustor film cooling or dilution flows. As such the freestream turbulence intensity and dissipation length scale were 1% and 0.1 m, respectively. The mass flow boundary conditions for the slot and the film-cooling holes were independently controlled and were placed at the entrance to large supply plenums for each.

The RANS, energy, and turbulence equations were computed until the residual values of the computations converged. The convergence of residuals for continuity, *x*-momentum, *y*-momentum, *z*-momentum, *k* and ε were resolved to levels of 10^{-4} with the exception of the energy equation which was set to a level of 10^{-7}. Typical computations required 1000 iterations for convergence to be met. Increasing the number of iterations by 10% resulted in a negligible change in effectiveness levels. After convergence, the mesh was then adapted based upon y^+ values, to insure values between $30 < y^+ < 60$, and velocity and temperature gradients. Typical unstructured mesh sizes consisted of 1.3×10^6 cells with the cells concentrated near the surfaces. Constraints on the y^+ values were met both in the film holes and in the passage. After adapting from a mesh size of 8.5×10^5 to 1.3×10^6 cells the area-averaged effectiveness predictions on the endwall were found to vary by only $\Delta\eta = \pm 0.005$ at a level of $\eta = 0.11$.

To validate the computational results, adiabatic endwall temperatures were measured for the case simulating the coolant flow leakage through a flush slot between the combustor and turbine. The vane and slot geometries were scaled up by a factor of nine to allow for good measurement resolution and, as such, that same scaling factor was applied for the computations. The experiments for this study were performed in a low speed, closed-loop wind tunnel facility previously described by Barringer et al [19] and Colban et al. [11]. This facility includes three channels including a heated primary channel, representing the main gas path, and two symmetric secondary channels, representing the coolant flow paths. Within the primary channel, the flow passes through a thermal and flow conditioning section containing a bank of heaters followed by a series of screens and flow straighteners. For the studies presented in this paper, the heaters were not used since a large enough temperature differential (25˚C) was achieved between the primary flow and coolant. This temperature differential was achieved by using chilled water in the heat exchangers located in the secondary flow channel. A 38 kW chiller was installed to insure large temperature differentials.

An infrared camera was used to measure adiabatic wall temperatures on the endwall surface. Measurements were taken at thirteen different viewing locations to insure that the entire endwall surface was mapped. Each picture covered an area that was 19.4 cm by 15.7cm with the area being divided into 255 by 206 pixel locations. The spatial integration for the camera was 0.37cm (0.0062 chords). At each viewing location five images were averaged with each image being averaged over 16 frames, which provided a total of 80 data points that were averaged at

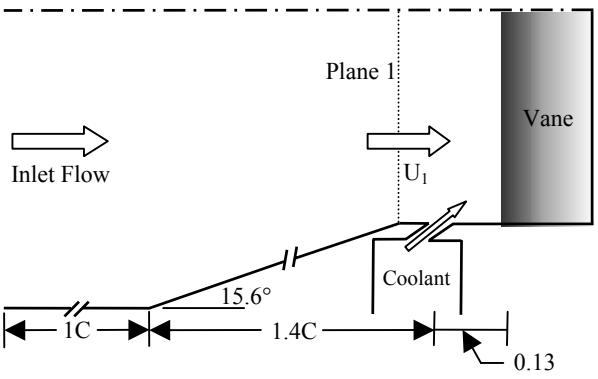

Figure 2a. A combustor contraction was modeled upstream of the slot and vane. A symmetry condition was applied at midspan.

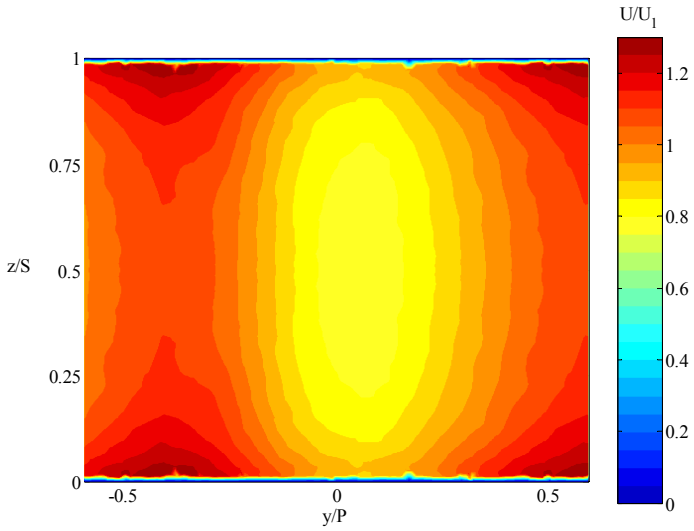

Figure 2b. The velocity distribution at the exit of the contraction (Plane 1) is shown normalized by the mass averaged velocity at the contraction exit.

each pixel location. Overlapping images were also averaged as the complete picture was assembled. Small shiny thumbtacks were embedded in the endwall as location markers to determine the orientation of the picture in a global coordinate system. Calibration of the infrared camera was completed using thermocouples embedded in the endwall along the passage.

The partial derivative and sequential perturbation methods, described by Moffat [20] were used to estimate the uncertainties of the measured values. Precision uncertainties were calculated based on a 95% confidence interval. The bias and precision uncertainties on the thermocouple measurements were 0.2˚C and 0.36˚C and on the IR camera measurements were 1˚C and 0.1˚C. As a result of these uncertainties, the adiabatic effectiveness uncertainty is $\eta = \pm 0.04$ at an $\eta = 0.4$.

DISCUSSION OF RESULTS

The results from the predictions made for the test cases shown in Table 2 will be discussed in a logical progression of complexity. First, the cooling provided from the leakage slot flow alone will be examined. Second, adiabatic effectiveness levels for the case with film-cooling alone for both endwall patterns will be discussed. Finally, the predictions for the combined slot and film-cooling configurations will be compared to the predictions for the slot alone and endwall film-cooling alone. The superposition method will be evaluated using the slot alone and endwall film-cooling alone as compared with the predictions for the combined slot and film-cooling configurations. Note that for all of the calculations, the density ratio (jet-to-mainstream) was held fixed at 1.14 to allow for comparisons with experiments.

Table 2. Computational and Experimental Test Matrix

	Slot flow $\%m_{exit}/M_{in}$	Film flow $\%m_{exit}/M_{in}$	Cooling Patterns	Discharge Coefficient
Case 1	0.5 / 0.18	- - -	- - -	- - -
Case 2*	1.0 / 0.37	- - -	- - -	- - -
Case 3a	- - -	0.5 /1.2	1	0.49
Case 3b	- - -	0.5 / 1.5	2	0.50
Case 4a	0.5 / 0.17	0.5 / 1.2	1	0.57
Case 4b	0.5 / 0.18	0.5 / 1.5	2	0.58
Case 5a	0.5 / 0.17	0.75 / 1.8	1	0.59
Case 5b	0.5 / 0.18	0.75 / 2.2	2	0.60

*Experimental data was also acquired for this case

Slot Injection at the Combustor-Turbine Interface

As previously discussed several cases were computed for a two-dimensional flush slot upstream of the turbine vane (cases 1 and 2 in Table 2). The predicted adiabatic effectiveness levels for the slot cooling, with the coolant flow being 1% of the exit mass flow, are shown in Figure 3a while the experimental measurements for the same case are shown in Figure 3b. Note that Figure 3b shows contours only downstream of the slot injection, which was limited by the optical access. As can be seen from Figures 3a and 3b, there is a general agreement between the trends in which the coolant exits the slot in a non-uniform manner and is swept towards the suction side-endwall junction. For both the computations and experiments there is a warm ring around the airfoil that extends from the stagnation location and along the entire pressure side. A large portion of the suction side also has a warm ring along the endwall in the vane-endwall juncture. The computational results indicate that at s/C = 0.65, the coolant from the slot

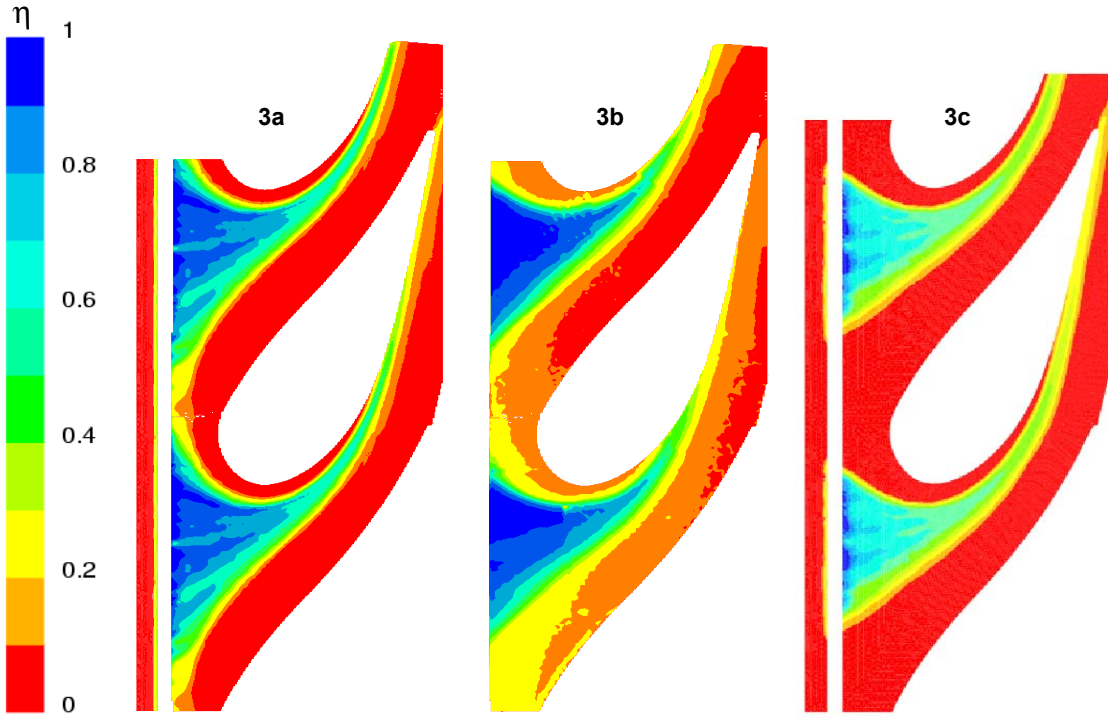

Figure 3a-c. Predicted (a) and measured (b) adiabatic effectiveness contours for 1% slot flow alone (case 2) and predicted (c) adiabatic effectiveness contours for 0.5% slot flow alone (case1).

impacts the suction side of the vane. Experimentally, this same phenomenon occurs at a position slightly further upstream along the suction side of the vane. The warm ring is a result of the horseshoe vortex that is wrapping around the vane as well as the large passage vortex that is convected toward the suction side of the vane. The coolant is lifted from the endwall surface by the upward velocity vectors of the secondary flow thereby reducing the cooling effectiveness on the endwall.

Figure 3c shows the predicted contours for the 0.5% coolant flow (case 1). There is a definite reduction in the predicted effectiveness levels for the 0.5% coolant flow as compared to the 1% coolant flow (case 2). There is essentially no coolant exiting the slot directly upstream of the vane stagnation for case 1. It is interesting that the coolant intersects the suction side at a position further downstream from the stagnation location.

Pitchwise averaged effectiveness levels predicted for the 0.5% and 1% cases and measured for the 1% case are shown in Figure 4. These averages indicate improved cooling for the higher coolant flow condition in the upstream endwall region. There is a large improvement in the leading edge region for the higher coolant flow condition. Progressing downstream, however, the two coolant flow conditions give approximately the same pitchwise-averaged effectiveness levels.

Cooling Hole Injection Along the Vane Endwall

Two cases were computed for the endwall cooling investigation, which included the two different endwall cooling hole patterns with each having 0.5% coolant injection. Note that there are 14 more cooling holes for the cooling hole configuration #1 as compared with #2, which was dictated by the designs given by industry (pattern #2 has 78% of the hole area of pattern #1). As a result of this disparity in the number of cooling holes, the coolant flow distribution is different for each of the hole patterns. The blowing ratios based on the inlet flow conditions (M_{in}) for patterns #1and #2 were 1.2 and 1.5, respectively.

As would be expected based on the iso-velocity contours there is a large variation in the local flow rate through each of the holes given that all of the holes are fed from a common plenum supply. The local blowing ratio (M) of a number of representative holes is listed in Tables 3a and 3b for the two hole patterns. Note that these are local blowing ratios rather than that based on the inlet velocity conditions (M_{in}). Of interest for this section of the paper is case 3a listed in Tables 3a and 3b. The locations of these holes, which are nearly paired between the two passages, are shown in Figure 1a. Tables 3a and 3b show that near the leading edge (holes 1.6 and 2.6) the blowing ratio is the lowest with a large discrepancy between the two cooling hole patterns. The large difference between the two hole patterns is attributed to the fact that there are fewer holes in pattern #2 as compared with pattern #1. One could predict the mass flow rate through the cooling holes using a known discharge coefficient and the total plenum to exit static pressure difference. Since the total flow through each of the holes is known from the CFD results, it was possible to deduce a representative discharge coefficient. These discharge coefficients are listed in Table 2 for the various cases. As the mass flow through the holes increases, so does the discharge coefficient. Figures 5a-5b present the predicted endwall effectiveness levels for the two cooling hole patterns. The computational results indicate that the injection from the cooling holes in the first streamwise row of holes remain

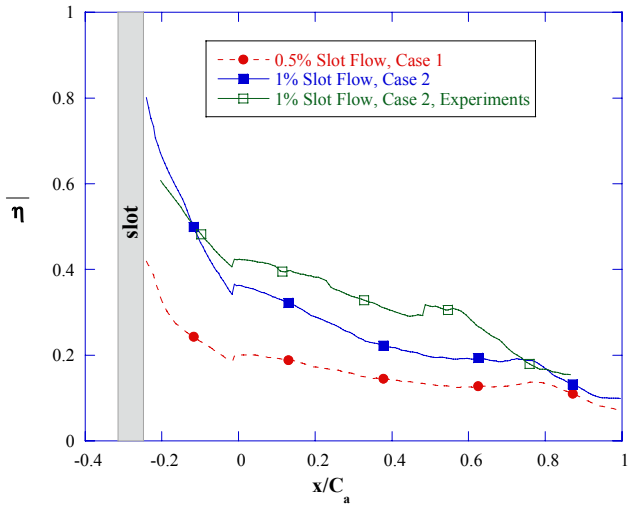

Figure 4. Pitchwise-averaged effectiveness levels through the vane passage for slot flow alone.

Table 3a. Film-Cooling Blowing Ratios for Pattern 1

Hole	Case 3a	Case 4a	Case 5a
1.1	0.82	0.92	1.59
1.2	1.22	1.42	1.95
1.3	2.37	2.77	3.07
1.4	0.70	0.89	1.58
1.5	0.86	0.90	1.55
1.6	0.33	0.33	1.27

Table 3b. Film-Cooling Blowing Ratios for Pattern 2

Hole	Case 3b	Case 4b	Case 5b
2.1	1.18	1.32	2.14
2.2	2.09	2.34	2.92
2.3	2.51	2.92	3.39
2.4	1.10	1.31	2.18
2.5	1.28	1.31	2.16
2.6	0.94	0.96	1.93

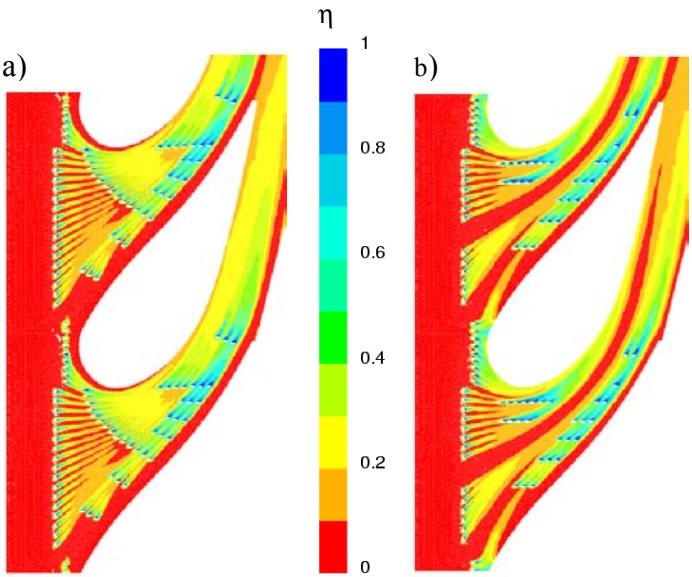

Figure 5a-5b. Predicted adiabatic effectiveness levels for 0.5% film flow with (a) hole pattern #1-case 3a; and (b) hole pattern #2-case 3b.

relatively discrete for pattern #1 (Figure 5a), particularly nearer to the suction side of the vane passage. Recall all of the holes in this first row are injecting towards the top of the picture, as was indicated in Figure 1b. Closer to the pressure side of the vane but still in the first row of holes, the jets are slightly more merged as a result of the sweeping motion of the passage vortex at this location. The endwall cooling along the pressure side of the airfoil is non-existent for pattern #1 as illustrated by the η = 0 contours in this region. The coolant injected from holes in the vane passage located near the pressure side of the airfoil is primarily blowing in the same direction as the streamlines even though these holes are directed towards the pressure surface. Relatively good cooling along most of the endwall, with the exception of the band near the pressure surface, is predicted for pattern #1 at a film-cooling flow rate of 0.5%.

There are a number of noticeable differences in the effectiveness levels for hole pattern #2 relative to pattern #1. For the cooling holes located just upstream of the vane stagnation, it is clear that the cooling is much more effective for hole pattern #2 as compared with hole pattern #1 even though the hole configuration at this location is the same for the two patterns. The reason for this better cooling is because there is proportionally a higher flow rate through the set of holes at the leading edge for the pattern #2 as compared with pattern #1 (see holes 2.6 and 1.6 in Tables 3a and 3b). The effectiveness contours are much cooler in the stagnation area extending along the suction side of the vane for pattern #2 as compared to pattern #1.

In the passage itself, the most noticeable difference between the two cooling hole patterns is that while relatively uniform coverage in the passage existed for hole pattern #1 (with the exception of near the pressure surface), the effectiveness contours for hole pattern #2 indicate the presence of a hot streak that travels down the mid-passage of the vane. This hot streak is a result of the break in the cooling hole placement due to the gutter that would be present in the region where adjacent vane platforms meet (discussed previously). Coolant exiting from the gutter could potentially alleviate these high temperatures, but if no coolant leaked out of the gutter region there would be damage to the endwall in this high temperature region.

Similar to pattern #1, the cooling from the first row of holes remains relatively discrete for the pitchwise row of holes injecting nearer to the suction side of the vane passage for pattern #2. For the first row holes in the mid-passage region of pattern #2, the coolant does not remain in discrete streaks, but rather merges into one large, cooler area. Also similar to pattern #1, there is no coolant present along the endwall close to the pressure side of the airfoil for pattern #2. In the case of hole pattern #2, the endwall cooling holes along the pressure side of the vane are injecting directly towards the vane. Although the coolant was not able to overcome the crossflows present resulting in a hot region along the pressure side, the overall cooling effectiveness levels downstream of the jet injection were higher than in the case for hole pattern #1 in this region.

Combined Slot and Film-Cooling Injection

Four cases were computed for the combined slot and film-cooling injection studies, which included the slot combined with the two hole patterns at two different film-cooling flow conditions. The slot flowrate remained fixed at 0.5% while the

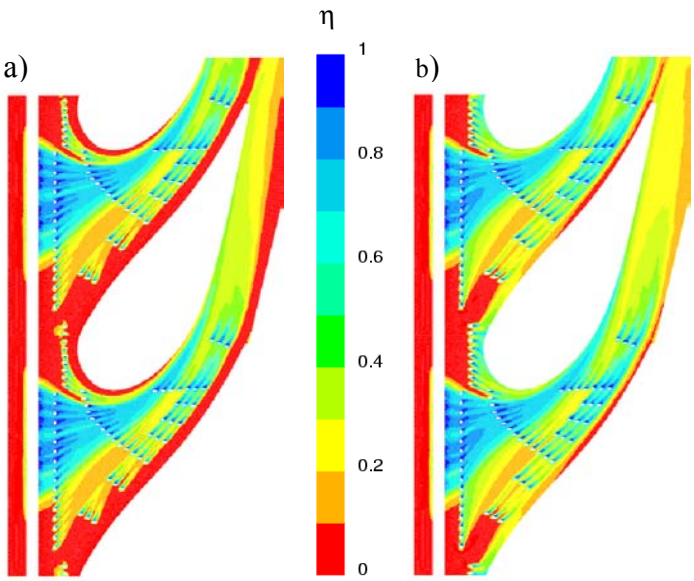

Figure 6a-6b. Predicted adiabatic effectiveness levels for combined film flow and slot flow with (a) hole pattern #1-case 4a; and (b) hole pattern #1-case 5a.

film-cooling flowrates considered were 0.5% (cases 4a and 4b) and 0.75% (cases 5a and 5b). Note that the slot and the film-cooling flow rates were set independently through the use of two different supply plenums. Tables 3a and 3b give the local blowing ratios for the hole locations indicated in Figure 1a. Note that all of the blowing ratios slightly increased for the combined film-cooling/slot cases for both hole patterns. The reason for this slight increase is because the exit mass flow through the vane was held fixed and, as such, relatively more coolant was sent through the holes since the slot flow was taken out of the mainstream flow. Other than the slightly higher blowing ratios, the relative difference between the cooling holes was nominally the same. Figures 6a-6b show the contour plots for the two flowrate conditions for the combined slot and cooling hole pattern #1. Figure 6a illustrates that the slot coolant contributes to the cooling effectiveness near the suction side of the airfoil and rather than discrete jets as was shown in Figure 5a, this region is relatively cooled uniformly. The trajectory of the cooling jets looks to be very similar for the endwall cooling alone as compared with the combined slot/endwall cooling configuration. The exit slot flow is also not effected by the downstream cooling hole injection.

There is a definite increase in the adiabatic effectiveness levels for the increased film-cooling flow as shown by Figure 6b. The leading edge holes indicate a much better performance with continued increases in effectiveness along the pressure side of the airfoil. The pressure side region showed the most dramatic increases in effectiveness with the increased coolant flow from the film-cooling holes. The trajectory of the cooling jets has changed significantly for the higher cooling flow case, particularly along the pressure side. Rather than being swept in the streamwise direction, these jets have enough momentum to penetrate closer towards the pressure side of the vane. There is also a slight improvement in effectiveness along the suction side of the vane.

For cooling hole pattern #2, shown in Figures 7a-7b at the two coolant flow conditions, the slot interaction with the cooling holes showed one noticeable effect. In the case with

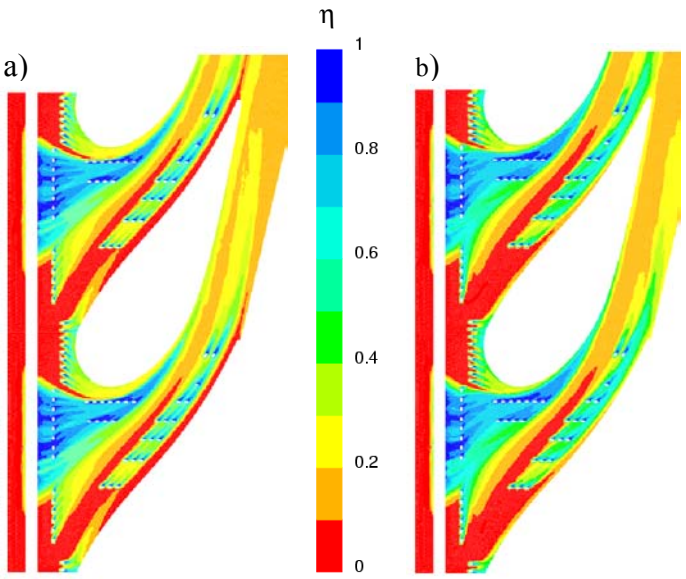

Figure 7a-7b. Predicted adiabatic effectiveness levels for combined film flow and slot flow with (a) hole pattern #2-case 4b; and (b) hole pattern #2-case 5b.

only endwall cooling, the jets exiting from the holes in the leading edge row near the mid-passage region were more directed toward the pressure side of the vane (Figure 5b) as compared to the predictions shown in Figure 7a. For the combined slot/hole configuration, Figure 7a shows that the leading edge jets in the mid-passage region are being entrained by the slot flow. This effect is even more dramatic at the higher cooling flow case shown in Figure 7b with the coolant from these jets being strongly turned toward the suction side of the adjacent vane.

For both coolant flow conditions in hole pattern #2, the hot streaks through mid-passage still remain for the combined slot/hole configuration. For the higher film-cooling flowrate shown in Figure 7b, there is a predicted increase in effectiveness levels as compared with the lower film-cooling flowrate shown in Figure 7a. The detriment at the higher blowing ratio for hole pattern #2 is that the hot streak becomes wider as shown in Figure 7b. The reason for this widening is because the jets are more directed towards the pressure surface. These results indicate that even with the presence of the gutter, it may not be possible to cool the entire hot streak region.

Figure 8a compares the pitchwise averaged effectiveness levels for the combined slot/hole configuration for hole patterns #1 and #2 at the two different film-cooling flowrates. For all of the cases, the averaged effectiveness levels agree just after the slot to $x/C_a = -0.15$. The peak in effectiveness level occurs just downstream of the slot for all of the cases with a second peak occurring for hole pattern #1 at $x/C_a = 0.6$. Downstream of the slot, the averages indicate the highest predicted effectiveness averages occur for hole pattern #1 at the higher coolant flow condition. There is a distinct increase in the pitchwise-averaged effectiveness levels for hole pattern #1 at the higher coolant flow condition. This is not the case for hole pattern #2, which indicates nearly the same pitchwise averaged effectiveness levels for the two coolant flow conditions. The reason for the lack of improved performance is because of the large hot streak in the mid-passage for hole pattern #2, which occurs at both the low and high coolant flow conditions.

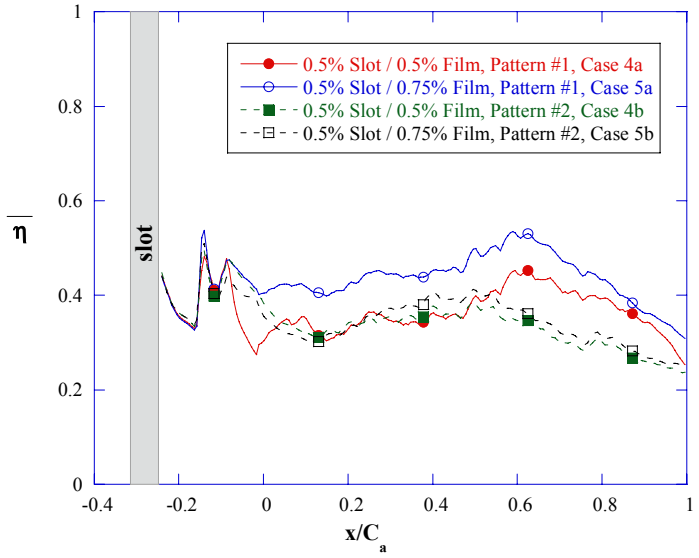

Figure 8a. Pitchwise-averaged effectiveness levels for the combined film-cooling and slot cooling

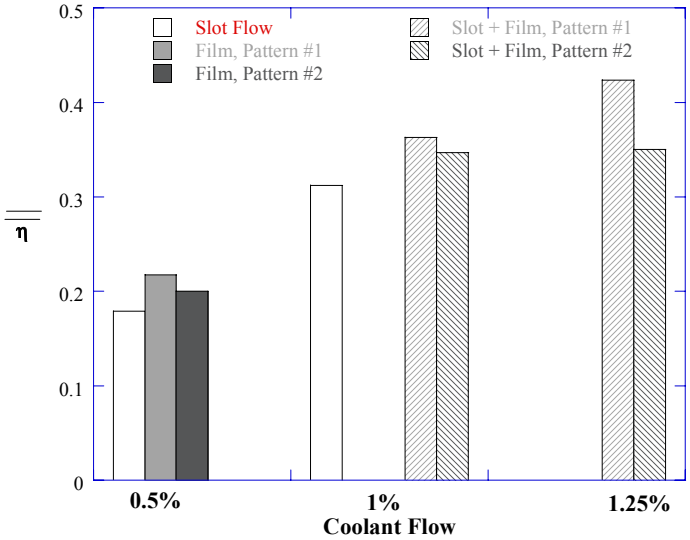

Figure 8b. Summary of area-averaged effectiveness values for all of the cases studied.

Figure 8b provides an overall summary of the area-averaged effectiveness levels for all of the cases evaluated. These area-averaged effectiveness levels can be used as a guide for designers in choosing whether coolant is more effectively used through the slot interface or through the cooling holes. Note that the areas for these cases were all computed based on the axial position located at the downstream edge of the slot. As a result of this fixed area, there is a large uncooled portion of the endwall upstream of the holes that brings down the area-averaged effectiveness levels. In all of the flow rates considered, pattern #1 was superior to pattern #2. It is also evident that increasing the flow rate from pattern #2 did not result in much benefit from an average endwall temperature perspective. Figure 8b also indicates that for the 0.5% coolant flow, it is beneficial from an average perspective to inject the coolant flow from the cooling holes alone rather than from the slot alone. One word of caution, however, is that the local variations without the slot cooling (such as upstream of the first

row of holes) may be too great and, as such, the area averaged effectiveness values alone do not tell the entire story.

An analysis was made based on the predicted effectiveness levels as to whether superposition may be appropriate in which effectiveness predictions for the slot alone and for the film-cooling holes alone could be combined to give an indication of the effectiveness levels for a case with a combined slot and film-cooling holes. Figure 9 shows the predictions made for each cooling element alone (slot or cooling holes), the two combined using superposition, and the directly predicted pattern #2 which was used for this exercise, the results are representative of what occurs for hole pattern #1 as well.

The pitchwise-averaged effectiveness values in Figure 9 indicate that there is a slight effect of the downstream film-cooling on the exit slot flow as indicated by the slightly lower averaged effectiveness just downstream of the slot. Progressing downstream of the slot, the predicted averaged effectiveness values are slightly higher than the superimposed values until $x/C_a = 0.15$. Downstream of this location, the superposition solution indicates higher values. In general, these results indicate that a superposition analysis can not be simply applied for the combined film-cooling and slot flows. Recall that superposition theory presumes that the flow field remains constant for the two solutions used in the analysis. As such, one potential reason for the inability to accurately use superposition theory for the combined slot and film-cooling flows is that the flow field has significantly changed for the combined slot and film-cooling case as compared with the slot alone and the film-cooling alone.

Secondary Flow Field Analysis

Secondary flow fields were analyzed at a number of locations throughout the vane passage. Presented here is only one flow field plane, which is near the exit of the vane passage and is normal to the pressure side of the vane (indicated by the line shown in Figure 1a at the trailing edge of the pressure surface). The secondary flow fields are plotted using vectors of V_n and V_z, as defined in the nomenclature, thereby representing the deviation of the flow relative to that for the mid-span inviscid flow. The view taken for the plots is looking upstream. Figures 10a-10d show the secondary flow vectors with superimposed thermal fields for the following cases: 0.5% slot flow alone (case 1), 0.5% film-cooling alone (case 3b), 0.5% film-cooling (case 4b) combined with 0.5% slot cooling, and 0.75% film-cooling combined with 0.5% slot cooling(case 5b). Since the secondary flow field results are similar between hole patterns #1 and #2, representative results will only be presented for hole pattern #2. These plots are for 15% of the span (z/S = 0.15) where y/P = 0 is located on the pressure side of the vane.

Figure 10a shows the typical passage vortex that is expected to occur in most turbine vane flows with a low slot flow condition. The vortex center is located near 5% of the span near mid-passage (y/P = 0.1). In contrast, Figure 10b indicates that with the film-cooling alone there is a strong cross-flow along the endwall, but the roll-up of the vortex is not as well-defined. The stronger cross-flow near the endwall is a result of the lower momentum fluid near the endwall that is present from the film-cooling injection as compared with the slot alone. The thermal fields in Figure 10b clearly show the existence of the gap in cooling along the endwall.

Figure 10c shows the secondary flow and thermal fields for the case with the combined slot and film-cooling flows. The

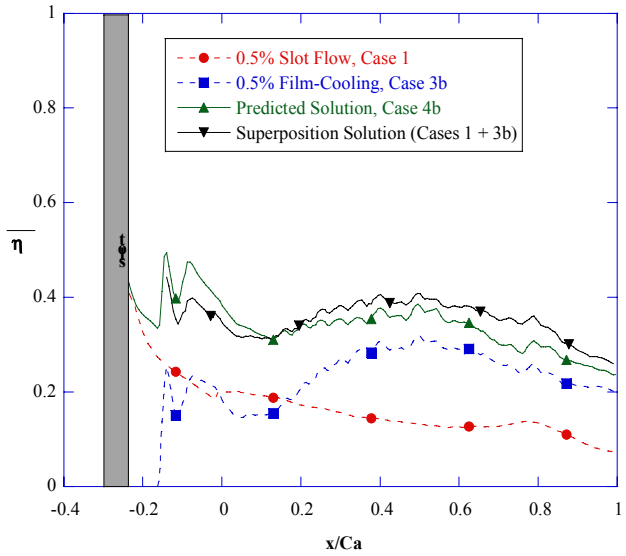

Figure 9. Comparison of predicted pitchwise-averaged effectiveness levels as compared with those calculated using the superposition for the 0.5% slot and 0.5% film-cooling flow cases with hole pattern #2.

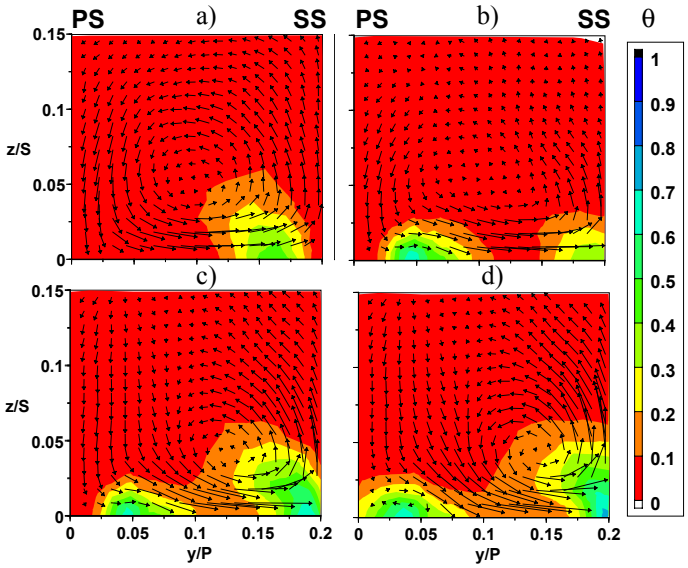

Figure 10a-10d. Secondary flow and thermal fields for the (a) slot cooling alone-case 1; (b) film-cooling alone-case 3b; (c) combined slot flow-and low film flow rate-case 4b; (d) combined film-cooling and slot flow at the higher film blowing ratio-case 5b. Cooling hole pattern #2 was used for these results.

secondary flow pattern for the combined cooling flows is the strongest relative to the slot or film-cooling alone. The vortex pattern has shifted toward the suction side of the vane and is closer to the endwall than that shown in Figures 10a and 10b. The thermal fields in Figure 10c indicate the slot coolant has helped fill the gap along the endwall compared to Figure 10b.

The case with the higher film-cooling injection is shown in Figure 10d indicating a stronger secondary flow pattern than that shown in Figure 10c. As the film-cooling flow is further increased, more of the coolant is convected up the suction side of the vane. The other noticeable difference is the spreading

apart of the two cool regions along the endwall. For the lower blowing case shown in Figure 10c, the peak effectiveness levels were located at y/P = 0.05 and y/P = 0.18 while for the higher blowing case shown in Figure 10d, the peak effectiveness levels were located at y/P = 0.03 and y/P = 0.2. This difference in the location of the effectiveness peaks between the two blowing ratios occurs as a result of the higher momentum jets for the higher blowing ratio case. In addition to the difference in peak locations, there is a greater spreading for the higher blowing ratio near the pressure side of the vane as indicated by comparing Figures 10d and 10c.

Based on these secondary flow patterns and the thermal field contours, it is not surprising that the superposition method is not viable for predicting the coolant effectiveness along the endwall for the slot flow alone and film-cooling flow alone to give the cooling effectiveness for the combined cooling methods. As was shown in Figure 9, an overprediction of effectiveness results through the use of the superposition method as compared with the predicted effectiveness levels.

CONCLUSIONS

The studies presented in this paper showed the effect of coolant injected from a two-dimensional slot at the combustor-turbine interface alone; endwall film-cooling alone; and combined slot and endwall film-cooling. The resulting endwall effectiveness from slot cooling alone showed a pattern that is quite non-uniform along the endwall with most of the coolant being swept toward the suction side of the vane. One could expect a burn-out near the vane-endwall juncture if only depending on the slot cooling from the combustor-turbine interface as a result of a warm ring extending most of the vane.

Placing film-cooling holes in the endwall is critical for increasing component life. The placement of these holes is difficult because the trajectory of the jets is not intuitive given the strong cross-flows that develop in the endwall region. The results of this study showed that the jet trajectory is highly dependent on the local blowing ratio for the cooling holes. One of the most significant findings was a lack of endwall film-cooling along the region where two turbine vanes are mated. While this region typically has a gutter with some leakage flow, it is particularly important that there is cooler leakage flow present since it provides cooling to the regions where the endwall film-cooling does not.

Combining the slot and film-cooling flows provided the best overall coverage for the endwall, but the warm ring around the vane was still present until a higher flow rate through the film-cooling flows was introduced. The higher flow rate provided a higher momentum for the pressure side film-cooling jets thereby allowing for a jet trajectory that approached the vane. One important finding was that there was a change in the secondary flows that developed for the combined film-cooling and slot flow studies as compared to the film-cooling alone and slot alone. This is important because this change in flow fields explained why the superposition method can not be used to predict the combined endwall film-cooling and slot cooling effectiveness levels. Moreover, using the superposition method resulted in an overprediction of cooling results thereby underpredicting component life.

ACKNOWLEDGMENTS

This publication was prepared with the support of the US Department of Energy, Office of Fossil Energy, National Energy Technology Laboratory. However, any opinions, findings, conclusions, or recommendations expressed herein are those of the authors and do not necessarily reflect the views of the DOE. The authors would also thank David Candelori (Pratt & Whitney), Ron Bunker (General Electric), and John Weaver (Rolls-Royce) for their input.

NOMENCLATURE

C	=	true chord of stator vane
C_a	=	axial chord of stator vane
$\dot{m}$	=	mass flowrate
M	=	mass flux ratio, $m = \rho_c U_c / \rho_\infty U_\infty$
P	=	vane pitch; hole pitch
P_o, p	=	total and static pressures
Re	=	Reynolds number defined as $Re = C U_\infty / \nu$
s	=	distance along vane from flow stagnation
S	=	span of stator vane
T	=	temperature
x, y, z	=	coordinates
U	=	velocity magnitude
Greek		
η	=	adiabatic effectiveness, $\eta = (T_\infty - T_{aw})/(T_\infty - T_c)$
θ	=	dimensionless temperature, $\theta = (T_\infty - T)/(T_\infty - T_c)$
ρ	=	density
ν	=	kinematic viscosity
Subscripts		
1	=	combustor/contraction exit
ave, —	=	pitchwise average at a given axial location
ave, ▬	=	area average from slot to trailing edge
aw	=	adiabatic wall
c	=	coolant conditions
inlet	=	inlet conditions
∞	=	freestream conditions

REFERENCES

[1] Friedrichs, S., Hodson, H. P. and Dawes, W. N., 1996, "Distribution of Film-Cooling Effectiveness on a Turbine Endwall Measured Using the Ammonia and Diazo Technique," *J of Turbomachinery*, **118**, pp. 613-621.

[2] Friedrichs, S., Hodson, H. P. and Dawes, W. N., 1997, "Aerodynamic Aspects of Endwall Film-Cooling," *J of Turbomachinery*, **119**, pp. 786-793.

[3] Friedrichs, S., Hodson, H. P. and Dawes, W. N., 1999, "The Design of an Improved Endwall Film-Cooling Configuration," *J of Turbomachinery*, **121**, pp. 772-780.

[4] Blair, M. F., 1974, "An Experimental Study of Heat Transfer and Film Cooling on Large-Scale Turbine Endwalls," *J of Heat Transfer*, pp. 524-529.

[5] Granser, D. and Schulenberg, T., 1990, "Prediction and Measurement of Film Cooling Effectiveness for a First-Stage Turbine Vane Shroud," 90-GT-95.

[6] Burd, S. W. and Simon, T. W., "Effects of Slot Bleed Injection over a Contoured Endwall on Nozzle Guide Vane Cooling Performance: Part I: Flow Field Measurements," 2000-GT-199.

[7] Burd, S. W., Satterness, C. J., and Simon, T. W., "Effects of Slot Bleed Ijection over a Contoured Endwall on Nozzle Guide Vane Cooling Performance: Part II Thermal Measurements," 2000-GT-200.

[8] Oke, R., Simon, T., Burd, S. W., Vahlberg, R., "Measurements in a Turbine Cascade Over a Contoured Endwall: Discrete Hole Injection of Bleed Flow," 2000-GT-214.

[9] Oke, R., Simon, T., Shih, T. Zhu, B., Lin, Y. L., Chyu, M. "Measurements Over a Film-Cooled, Contoured Endwall with Various Coolant Injection Rates," 2001-GT-140.

[10] Roy, R. P., Squires, K. D., Gerendas, M., Song, S., Howe, W. J., and Ansari, A., " Flow and Heat Transfer at the Hub Endwall of Inlet Vane Passages-Experiments and Simulations," 2000-GT-198.

[11] Colban, W. F., Thole, K. A., and Zess, G., 2002, "Combustor-Turbine Interface Studies: Part 1: Endwall Measurements," GT-2002-30526.

[12] Colban, W. F., Lethander, A., T., Thole, K. A., and Zess, G., 2002, "Combustor-Turbine Interface Studies: Part 2: Flow and Thermal Field Measurements," GT-2002-30527.

[13] Kost, F. and Nicklas, M., 2001, "Film-Cooled Turbine Endwall in a Transonic Flow Field: Part I – Aerodynamic Measurements," 2001-GT-0145.

[14] Nicklas, M., 2001, "Film-Cooled Turbine Endwall in a Transonic Flow Field: Part II – Heat Transfer and Film-Cooling Effectiveness Measurements," 2001-GT-0146.

[15] Radomsky, R. W., and Thole, K. A., 2000, "Flowfield Measurements for a Highly Turbine Flow in a Stator Vane Passage," *J of Turbomachinery*, **122**, pp. 255-262.

[16] Harasgama, S. P., and Burton, C. D., 1992, "Film Cooling Research on the Endwall of a Turbine Nozzle Guide Vane in a Short Duration Annular Cascade: Part 1— Experimental Technique and Results," *J of Turbomachinery*, **114**, pp. 734-540.

[17] Fluent Inc., Version 6.0, 2002 (Fluent Inc: New Hampshire).

[18] Hermanson, K., and Thole, K.A., 2000, "Effect of Inlet Profiles on Endwall Secondary Flows," *Journal of Propulsion and Power,* **16**, pp 286-296.

[19] Barringer, M. D., Richard, O. T., Walter, J. P., Stitzel, S. M., and Thole, K. A., 2002, "Flow Field Simulations of a Gas Turbine Combustor," *J of Turbomachinery*, **124**, pp. 508-516.

[20] Moffat, R. J., 1988, "Describing the Uncertainties in Experimental Results," *Experimental Thermal and Fluid Science*, **1**, pp. 3-17.